

Current-voltage calculations for InAs/AlSb resonant-tunneling diodes

Timothy B. Boykin

Department of Electrical and Computer Engineering, The University of Alabama in Huntsville, Huntsville, Alabama 35899

(Received 30 September 1994)

One expects that the one-dimensional approximation for the resonant-tunneling-diode tunneling current should be very accurate in the InAs/AlSb materials system, with its large barriers and largely Γ -like tunneling. We study this approximation as well as the two-dimensional expression, which takes into account the explicit dependence of the transmission coefficient on the magnitude of the in-plane wave vector \mathbf{k}_{\parallel} . We find that even here the one-dimensional approximation fails, producing curves that are qualitatively very different from those of the two-dimensional approximation and study the reasons for the differences. We also briefly examine the angular dependence of the transmission coefficients, the results indicating that the two-dimensional approximation is likely to be fairly good for the structures studied.

I. INTRODUCTION

Resonant-tunneling diodes (RTD's), quantum wells (QW's), and related structures formed by alternating thin layers of different materials are approximate realizations of the ideal, one-dimensional, double-barrier tunneling and particle-in-a-box problems familiar from introductory quantum mechanics. The realization is, however, an imperfect one for, even ignoring phonons, interface roughness, and imperfections, these devices are fully three dimensional, so that the carrier wave vector lying in the plane of the heterointerfaces, \mathbf{k}_{\parallel} , is a conserved quantity. The importance of nonzero \mathbf{k}_{\parallel} has long been recognized for hole and interband tunneling devices and QW's, owing to the presence of heavy-hole, light-hole, and split-off valence bands.¹ Recently, Kiledjian *et al.*² have calculated current-voltage characteristics for interband tunneling structures both with and without explicit \mathbf{k}_{\parallel} dependence, finding markedly different results in the two cases. In contrast, most models of conduction-band devices omit this \mathbf{k}_{\parallel} dependence, even though it was included long ago in the work of Ben Daniel and Duke.³ Apparently, many workers still believe that nonzero \mathbf{k}_{\parallel} is of little importance in conduction-band-only RTD's and QW's; here we show that this assumption is false.

While our previous work⁴ shows the importance of nonzero \mathbf{k}_{\parallel} for the transmission coefficients of InAs/AlSb RTD's, the most convincing demonstration remains a comparison of current-density-voltage (J - V) characteristics calculated with and without the explicit \mathbf{k}_{\parallel} dependence for ordinary devices fabricated in this materials system. The InAs/AlSb system is particularly attractive for this purpose due to the large conduction-band discontinuities between the Γ and X valleys of AlSb and the Γ valley of InAs, about 2.1 and 1.5 eV, respectively.⁵ (Here we consider structures having the growth axis along \mathbf{e}_z so that only the Γ and longitudinal X valleys are of concern in typical devices under the assumptions laid out in the foregoing paragraph.) As a consequence of these very large conduction-band offsets, flatband states tend to be

mostly Γ like except in the thinnest of structures,⁶ so that a RTD with an InAs well and bulk regions and AlSb barriers seems the realization of the one-dimensional double-barrier tunneling problem. Furthermore, this system is of technological importance: InAs/AlSb RTD's have demonstrated high peak-to-valley current ratios and large current densities, properties desirable for excellent high-frequency performance.⁷ Also, Carnahan *et al.*⁸ recently reported interesting magnetotunneling results on InAs/AlSb RTDs, and Brar *et al.*⁹ present photoluminescence results on very narrow InAs/AlSb QW's. Hence the attraction of this system for the study of the influence of nonzero \mathbf{k}_{\parallel} in calculated RTD J - V characteristics.

The paper is organized as follows. Section II discusses the method and assumptions employed. In Sec. III we present the results of our calculations and analyze them. Finally, Sec. IV contains the summary and our conclusions.

II. METHOD AND ASSUMPTIONS

We contemplate here a RTD grown in the z direction, having heterointerfaces parallel to the x - y plane, and ignore scattering due to phonons, interface roughness, impurities, and the like. As we study InAs/AlSb RTD's, we shall be concerned with electron tunneling only, and we denote by $-e$ the electron charge and V the bias across the device (for forward bias $V > 0$). (We ignore any interband tunneling which might occur at high bias when the quasi-Fermi level of the collector falls below the bulk emitter valence-band maximum.) With these assumptions and definitions, the conserved quantities are the energy E and in-plane wave vector $\mathbf{k}_{\parallel} = k_x \mathbf{e}_x + k_y \mathbf{e}_y$. Working within the single-electron approximation, we denote by $T(E, \mathbf{k}_{\parallel}, V)$ the transmission coefficient of an electron of energy E and in-plane wave vector \mathbf{k}_{\parallel} incident on a RTD under bias V . The magnitude of the net tunneling current from emitter to collector (including a factor of 2 for spin degeneracy) is then

$$J_3 = \frac{2e}{(2\pi)^3 \hbar} \int \int \int [f_e(E, V) - f_c(E, V)] \times T(E, \mathbf{k}_{\parallel}, V) d\mathbf{k}_{\parallel} dE, \quad (1)$$

where f_e and f_c are the Fermi-Dirac functions for the bulk emitter and collector, respectively (both presumed heavily doped). Because of the computational effort required to evaluate (1) numerically, one commonly makes one of two approximations to render the calculation more tractable.

The first level of approximation, which we shall call the two-dimensional approximation, results from the replacement

$$T(E, \mathbf{k}_{\parallel}, V) \rightarrow T(E, k_{\parallel} \mathbf{e}_x, V) \quad (2)$$

in (1), yielding

$$J_2 = \frac{2e}{(2\pi)^2 \hbar} \int \int [f_e(E, V) - f_c(E, V)] \times T(E, k_{\parallel} \mathbf{e}_x, V) k_{\parallel} dk_{\parallel} dE. \quad (3)$$

In (2) we assume that the transmission T is independent of the *direction* of \mathbf{k}_{\parallel} ; the choice $\mathbf{k}_{\parallel} = k_{\parallel} \mathbf{e}_x$ is made strictly for convenience. Note that if the transmission is indeed completely isotropic, then the two-dimensional approximation (3) is exact.

The second, very widely employed approximation to (1), which we shall term the one-dimensional approximation, results from replacing

$$T(E, \mathbf{k}_{\parallel}, V) \rightarrow T(E_z, 0, V) = T(E, V) \quad (4)$$

in (1), where $E_z = E - \hbar^2 k_{\parallel}^2 / 2m^*$, with m^* the electron effective mass in the bulk emitter, resulting in

$$J_1 = \frac{em^* k_B T}{2\pi^2 \hbar^3} \times \int T(E, V) \ln \left[\frac{1 + \exp \left[\frac{(\mu_e - E)}{k_B T} \right]}{1 + \exp \left[\frac{(\mu_e - E - eV)}{k_B T} \right]} \right] dE, \quad (5)$$

where T is the absolute temperature, k_B is Boltzmann's constant, and μ_e is the chemical potential in the bulk emitter. Note that (4) assumes that the transmission does not depend explicitly on \mathbf{k}_{\parallel} and is only exact should this be the case. Equation (5) is still widely used, doubtless due to its computational convenience, in spite of the fact that it can produce J - V characteristics having unphysical features.¹⁰

In this work we calculate the transmission coefficients with an empirical tight-binding approach (we employ the sp^3s^* nearest-neighbor model of Vogl, Hjalmarsen, and Dow¹¹) based on the transfer-matrix method;¹² the parameters used are listed in the Appendix. Due to the presence of evanescent transfer-matrix eigenstates, it is necessary to employ a numerical stabilization procedure for all but the shortest of structures. The details of our

method are presented elsewhere;¹³ other methods are also possible.¹⁴ We ignore the effects of strain in InAs/AlSb devices, taking the AlSb in-plane lattice constant to be that of InAs, and assume that there is associated with each AlSb barrier one InSb-type and one AlAs-type interface.¹⁵ We include space-charge regions in the calculation (Kiledjian *et al.*² do not), incorporating the Poisson solution into the Schrödinger equation as a stepwise-constant potential, but do not solve the two equations self-consistently.¹⁶ The numerical integration routine employs adaptive stepsize control.¹⁷

III. RESULTS AND DISCUSSION

Here we examine the two approximations to (1), given in Eqs. (2)–(5). Computer speed limitations render the evaluation of (1) highly impractical, so we will compare (3) and (5). We will also investigate the accuracy of (2) and (3) by examining the angular dependence of the transmission coefficients for the structures of concern.

In Figs. 1–5 we present the J - V and transmission characteristics of a double-barrier InAs/AlSb RTD with 13-monolayer (ML) undoped AlSb barriers and a 15-ML undoped InAs well. Between the emitter barrier and bulk emitter there are 33 ML of undoped InAs; on the collector side there is but 1 ML. Both bulk regions are N-doped to 10^{18} cm^{-3} , the temperature is 4.2 K, and each bulk chemical potential lies about 159 meV above its respective conduction-band minimum. In the calculation, we take each bulk region to be 450 ML in length to ensure a flat bulk conduction band.

Figure 1 shows the J - V curves of this device as calculated with the two-dimensional approximation (3) (solid line) and the one-dimensional approximation (5) (dashed line); symbols (diamonds and crosses, respectively) show the actual points computed. Obviously the two curves are very different, the two-dimensional result having a more gradual cutoff than the one-dimensional curve as well as a lower peak current density. The shape of the

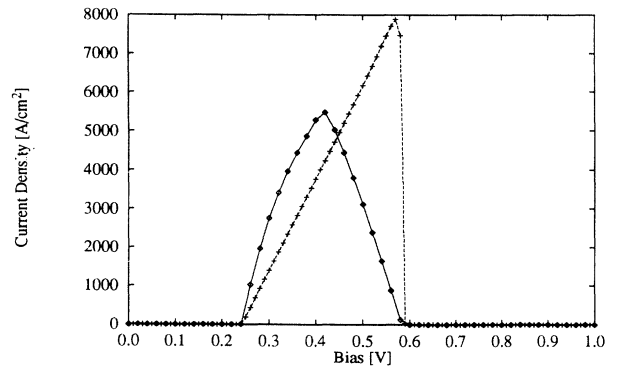


FIG. 1. Current density vs applied bias for an InAs/AlSb double-barrier RTD with 13-ML barriers and a 15-ML well as calculated using (3) (solid line) and (5) (dashed line). Actual points computed are indicated by diamonds and crosses, respectively.

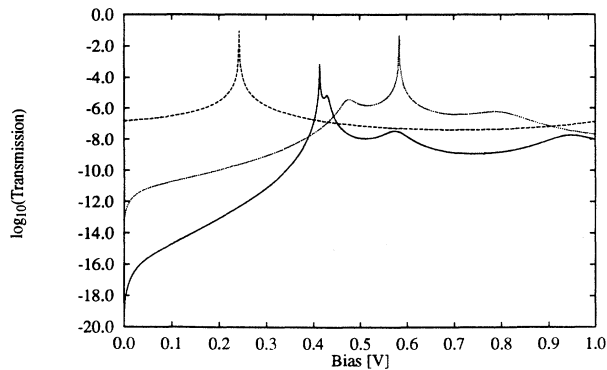


FIG. 2. Base-10 logarithms of the transmission coefficient vs applied bias for the device of Fig. 1. Solid line: $k_{\parallel}=0.04028 \text{ \AA}^{-1} \mathbf{e}_x$, $E \approx 0.15864 \text{ eV}$; dashed line: $\mathbf{k}_{\parallel}=\mathbf{0}$, $E \approx 0.15857 \text{ eV}$; dotted line: $\mathbf{k}_{\parallel}=\mathbf{0}$, $E \approx 1.430 \times 10^{-4} \text{ eV}$.

one-dimensional curve is easily understood in terms of a constant-width Lorentzian transmission model;¹⁰ we discuss the shape of the two-dimensional result below.

In spite of the qualitative differences between the two graphs, note that both have approximately the same turn-on and turn-off biases. The reasons for this become clear upon examination of the transmission coefficients in Fig. 2. At the turn-on bias, the main contributors to the tunneling current will be those electrons with maximum k_z in the bulk emitter. From the graph for the electron with bulk emitter wave vector $\mathbf{k}=k_f \mathbf{e}_z$ (k_f is approximately the Fermi wave vector) in Fig. 2 (dashed line) we see that this is indeed the case, for the transmission resonance occurs very near the turn-on bias. Similarly, the

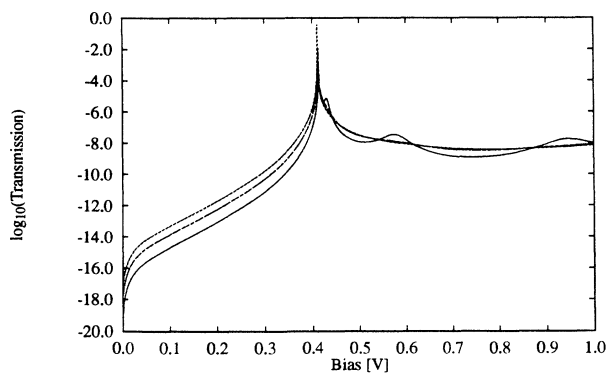


FIG. 3. Base-10 logarithms of the transmission coefficient vs applied bias for the device of Fig. 1. $k_{\parallel}=0.04028 \text{ \AA}^{-1}$, $E \approx 0.15864 \text{ eV}$ for various directions of \mathbf{k}_{\parallel} (see text). Solid line: $\theta=0$; heavy dashed line: $\theta=0.1\pi$; dotted line: $\theta=0.3\pi$; dashed-dotted line: $\theta=0.6\pi$; light dashed line: $\theta=0.8\pi$. Those for 0.3π and 0.8π lie nearly atop one another, as do those for 0.1π and 0.6π . At 0.1-V bias the highest transmission is at 0.3π and 0.8π , the lowest is 0, and those for 0.1π and 0.6π are in between.

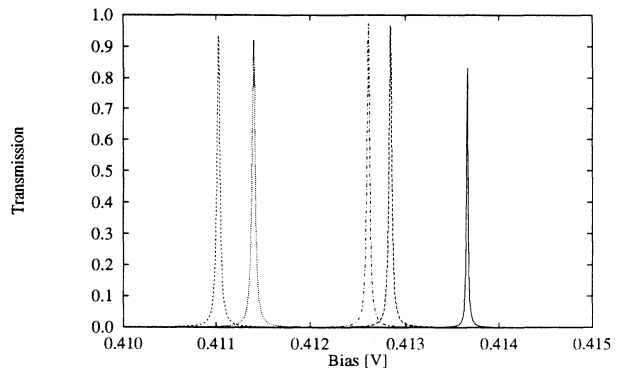


FIG. 4. Transmission coefficients of Fig. 3, plotted in the neighborhood of the peaks. Solid line: $\theta=0$; heavy dashed line: $\theta=0.1\pi$; dotted line: $\theta=0.3\pi$; dashed-dotted line: $\theta=0.6\pi$; light dashed line: $\theta=0.8\pi$.

main contributors at the turn-off bias will be those electrons with minimal k_z in the bulk emitter. Curiously, we see in Fig. 2 that the transmission of the electron with bulk emitter wave vector $\mathbf{k}=k_s \mathbf{e}_z$ (dotted line; we take a conveniently small value $k_s=0.001 \text{ \AA}^{-1}$) maximizes near the turn-off bias, but that the transmission of the electron with bulk emitter wave vector $\mathbf{k}=k_f \mathbf{e}_x + k_s \mathbf{e}_z$ (solid line) maximizes at a lower bias, in contrast to what we expect from effective-mass models. In earlier work⁴ we have shown that in InAs/AlSb devices the transmission peaks for electrons with a given bulk emitter E_z but larger k_{\parallel} tend to occur at lower biases than those of smaller k_{\parallel} , due to the nonparabolicity of the InAs conduction band: this separation of transmission peaks has a direct bearing on the shape of the two-dimensional result. Finally, the very-low bulk emitter k_z electrons show extra, very weak (note that logarithmic scale) transmission resonances.

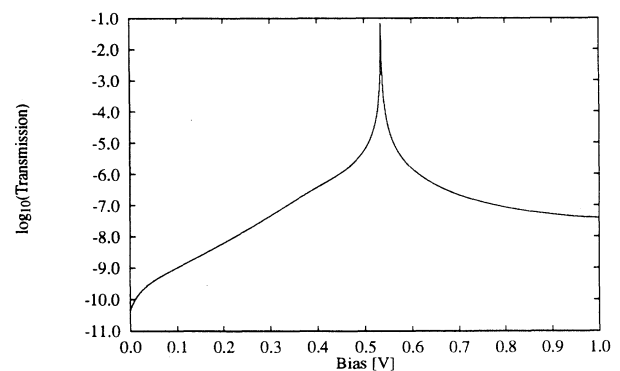


FIG. 5. Base-10 logarithms of the transmission coefficient vs applied bias for the device of Fig. 1. $k_{\parallel}=0.01 \text{ \AA}^{-1}$, $E \approx 0.02652 \text{ eV}$ for various directions of \mathbf{k}_{\parallel} (see text). Solid line: $\theta=0$; heavy dashed line: $\theta=0.1\pi$; dotted line: $\theta=0.3\pi$; dashed-dotted line: $\theta=0.6\pi$; light dashed line: $\theta=0.8\pi$. All curves lie nearly atop one another.

This is hardly surprising: from elementary wave considerations, we know that these electrons are very sensitive to minor potential hills and valleys which develop in the space-charge regions, such as the notch which usually forms in front of the emitter barrier. Thus their transmission will tend to show shallow peaks when they are in resonance with one of the very weakly bound above-notch states.

Let us now consider the shape of the two-dimensional graph. From Fig. 2, it is apparent that transmission resonance of the electron with bulk emitter $\mathbf{k} = k_f \mathbf{e}_x + k_s \mathbf{e}_z$ occurs at approximately the current-density peak; this can be explained with a simple counting argument. Notice that the transmission resonances for the electrons with bulk emitter $\mathbf{k} = k_f \mathbf{e}_z$ and $\mathbf{k} = k_s \mathbf{e}_z$ occur at lower and higher biases, respectively, so that the transmission of an electron with bulk emitter z -wave vector between these two should maximize at the current-peak bias as well (here $\mathbf{k} \approx 0.025 \text{ \AA}^{-1} \mathbf{e}_z$). Furthermore, this bias should coincide with the transmission resonance of electrons of all occupied k_{\parallel} and different bulk emitter k_z . Therefore, the greatest number of electrons contribute to the current at this bias and, discounting differences in transmission maxima and widths, the current tends to maximize here.

We now investigate the accuracy of the replacement (2) which results in the two-dimensional approximation (3) for this device by comparing transmission coefficients for incident electrons with the same k_{\parallel} and E but differing directions of \mathbf{k}_{\parallel} . In Fig. 3 we plot the transmission for electrons with $k_{\parallel} = 0.04028 \text{ \AA}^{-1}$ and energy relative to the bulk emitter conduction-band minimum, $E \approx 0.15864 \text{ eV}$ (i.e., near the Fermi surface in the bulk emitter) for several angles θ where $\mathbf{k}_{\parallel} = k_{\parallel} \cos(\theta) \mathbf{e}_x + k_{\parallel} \sin(\theta) \mathbf{e}_y$. In Fig. 4 we plot the same transmission coefficients on a linear scale in the neighborhood of the peaks. From Figs. 3 and 4 we see that the various peak biases differ by less than 3.5 mV and that there is some variation in the resonance widths. The $\theta = 0$ curve of Fig. 3 shows some extra, very shallow, transmission resonances, but its bulk emitter $k_z = 0.001 \text{ \AA}^{-1}$, whereas the values for the other electrons are about 0.00365 ($0.1\pi, 0.6\pi$) and 0.00577 \AA^{-1} ($0.3\pi, 0.8\pi$), so that it will more greatly feel the effects of band bending in the emitter space-charge region (recall the problem of transmission over a potential well from elementary quantum mechanics). In Fig. 5 we plot the transmission for electrons with $k_{\parallel} = 0.01 \text{ \AA}^{-1}$ and energy relative to the bulk emitter conduction-band minimum, $E \approx 0.02652 \text{ eV}$ (all have bulk emitter $k_z \approx 0.01 \text{ \AA}^{-1}$) for various directions of \mathbf{k}_{\parallel} . Here the agreement is much better, the curves lying almost atop one another. If the replacement (2) were exact, then all curves in Figs. 3–5 would exactly coincide. Notice, however, that even in Figs. 3 and 4 they are fairly close in position, while they are very close indeed in Fig. 5. Comparing the transmission behavior with that for a similar device studied earlier,⁴ we see that the replacement (2) is much better than the replacement (4). Thus, while Figs. 3–5 make it clear that (3) is not exactly correct for this device, they do indicate that it is probably a fairly good approximation; in any event it appears to be a reasonable

tradeoff between accuracy and computational effort *vis à vis* (1).

In Figs. 6–9 we consider the J - V and transmission characteristics of another InAs/AlSb RTD. This device has a 30-ML undoped InAs well and only 1 ML undoped emitter and collector spacers; the other parameters of this device are identical to those of the first. The J - V characteristics are qualitatively similar to their counterparts in Fig. 1, although the first peaks of both curves have immediate turn on and that of the two-dimensional result has a sharper cutoff. The reasons for this behavior are evident from Fig. 7, where we plot the transmission coefficients of three different electrons with in-plane wave vectors and energies (relative to the conduction-band minimum) $\mathbf{k}_{\parallel} = 0.04028 \text{ \AA}^{-1} \mathbf{e}_x \approx k_f \mathbf{e}_x$, $E \approx 0.15864 \text{ eV}$ (solid line); $\mathbf{k}_{\parallel} = 0$, $E \approx 0.15857 \text{ eV}$ (dashed line); and $\mathbf{k}_{\parallel} = 0$, $E \approx 6.767 \times 10^{-5} \text{ eV}$ (dotted line). The z energy of the first is identical to that of the last: $E - E_c(0.04028 \text{ \AA}^{-1} \mathbf{e}_x) \approx 6.767 \times 10^{-5} \text{ eV}$. We see that the transmission peaks of the second electron, which has a high bulk emitter k_z , coincide with the turn-on points at about 0.27 and 0.69 V. Notice, however, that this electron has no peak at zero bias: the first quasi-bound state for $\mathbf{k}_{\parallel} = 0$ lies below the bulk-emitter Fermi level. (Specifically, at zero bias, the electron with $\mathbf{k}_{\parallel} = 0$ and $E \approx 0.152 \text{ eV}$ is in resonance with the lowest quasi-bound state of the well.) The sharp cutoff of the first peak and gradual cutoff of the second are mirrored in the transmission plots as well: the lowest transmission resonances of the small- k_z electrons occur much closer together than do the second resonances. (Note that the InAs conduction band is less parabolic at the higher energies of the second transmission maxima.) Finally, as before, the transmission peaks of the electron with $\mathbf{k}_{\parallel} \approx k_f \mathbf{e}_x$ and small bulk emitter k_z approximately coincide with the current peaks of the two-dimensional result, while the transmission maxima of the electron with $\mathbf{k}_{\parallel} = 0$ and small bulk emitter k_z lie close to the cutoff points.

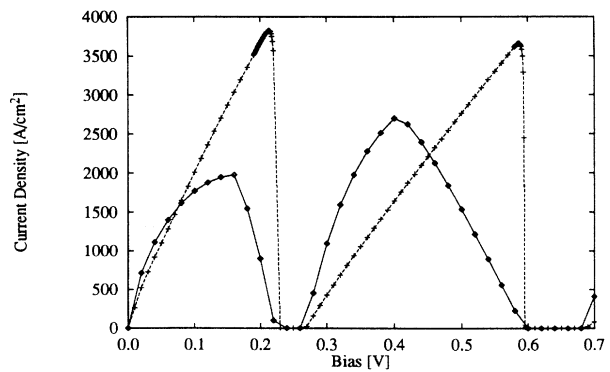


FIG. 6. Current density vs applied bias for an InAs/AlSb double-barrier RTD with 13-ML barriers and a 30-ML well as calculated using (3) (solid line) and (5) (dashed line). Actual points computed are indicated by diamonds and crosses, respectively.

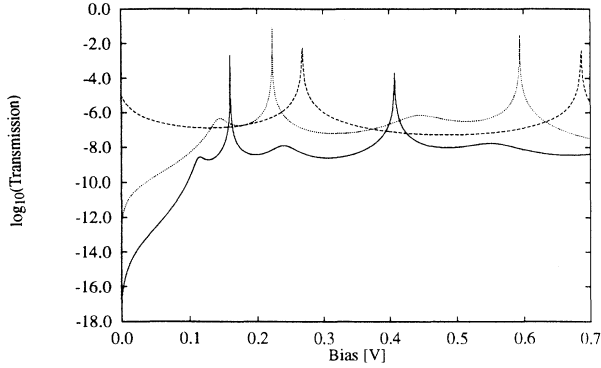


FIG. 7. Base-10 logarithms of the transmission coefficient vs applied bias for the device of Fig. 6. Solid line: $\mathbf{k}_{\parallel} = 0.04028 \text{ \AA}^{-1} \mathbf{e}_x$, $E \approx 0.15864 \text{ eV}$; dashed line: $\mathbf{k}_{\parallel} = 0$, $E \approx 0.15857 \text{ eV}$; dotted line: $\mathbf{k}_{\parallel} = 0$, $E \approx 6.767 \times 10^{-5} \text{ eV}$.

In Fig. 8 we demonstrate the inadequacy of the one-dimensional approximation (5) for this device. Here all of the electrons are of the same z energy, $E_z \equiv E - E_c(\mathbf{k}_{\parallel})$, in the bulk emitter; these energies and in-plane wave vectors are given in Table I. Were the replacement (4), which leads to the one-dimensional approximation (5), correct, all of the curves would exactly coincide. Observe that there is a significant spreading of even the first transmission maxima. As previously mentioned, this behavior arises from the nonparabolic InAs conduction band;⁴ in fact, it is not difficult to show that, under conditions which are usually obtained, increasing k_{\parallel} results in a lower resonant bias. Assume that the flatband quasi-bound state of interest lies below the inflection point of the conduction band, and that in the relevant energy range this band is describable by the isotropic, but nonparabolic form¹⁸

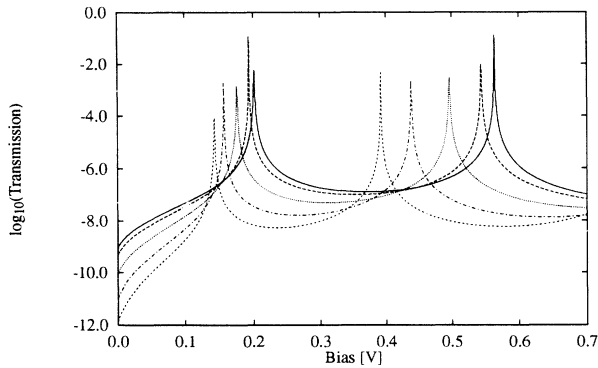


FIG. 8. Base-10 logarithms of the transmission coefficient vs applied bias for the device of Fig. 6. See Table I for the parameters of each curve: *A* (solid line), *B* (heavy dashed line), *C* (dotted line), *D* (dashed-dotted line), and *E* (light dashed line). In each group of transmission peaks the resonant bias *decreases* on progressing from curve *A* through curve *E*.

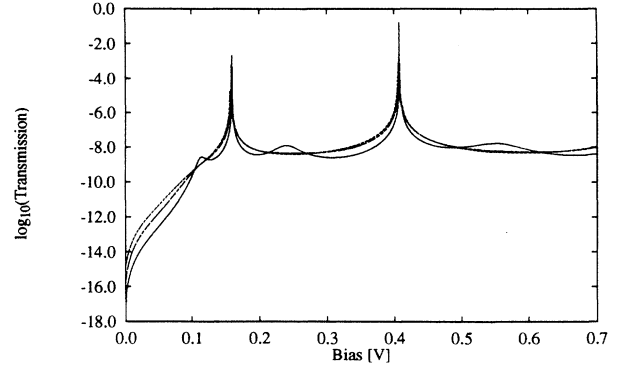


FIG. 9. Base-10 logarithms of the transmission coefficient vs applied bias for the device of Fig. 6. $k_{\parallel} = 0.04028 \text{ \AA}^{-1}$, $E \approx 0.15864 \text{ eV}$ for various directions of \mathbf{k}_{\parallel} (see text). Solid line: $\theta = 0$; heavy dashed line: $\theta = 0.1\pi$; dotted line: $\theta = 0.3\pi$; dashed-dotted line: $\theta = 0.6\pi$; light dashed line: $\theta = 0.8\pi$. Those for 0.3π and 0.8π lie nearly atop one another, as do those for 0.1π and 0.6π . At 0.05-V bias the highest transmission is at 0.3π and 0.8π , the lowest is at 0 , and those for 0.1π and 0.6π are in between.

$$E(1 + \alpha E) = \frac{\hbar^2 k^2}{2m^*}, \quad (6)$$

where $k^2 = k_{\parallel}^2 + k_z^2$. The relation $E(k)$ is then given by the solution of the quadratic equation (6), taking the positive square root. As long as the energy of the quasi-bound state relative to the conduction-band minimum at the center of the well is unchanged by applied bias, and the z -wave vector of this state, k_w , is the same for all k_{\parallel} or increases with increasing k_{\parallel} (these conditions were found to usually hold in Ref. 4), the bias at midwell necessary to bring the quasi-bound well state in resonance with the bulk emitter state $\mathbf{k} = k_{\parallel} + k_e \mathbf{e}_z$ is $U = E(\mathbf{k}_{\parallel} + k_w \mathbf{e}_z) - E(\mathbf{k}_{\parallel} + k_e \mathbf{e}_z)$, where we assume $k_e < k_w$, so that

$$\frac{\partial U}{\partial k_{\parallel}} = \frac{\hbar^2 k_{\parallel}}{m^*} \left[\frac{1}{\left[1 + \frac{2\hbar^2 \alpha}{m^*} (k_{\parallel}^2 + k_w^2) \right]^{1/2}} - \frac{1}{\left[1 + \frac{2\hbar^2 \alpha}{m^*} (k_{\parallel}^2 + k_e^2) \right]^{1/2}} \right] \quad (7)$$

TABLE I. Values of in-plane wave vector, $\mathbf{k}_{\parallel} = k_x \mathbf{e}_x$, and energy relative to the bulk emitter conduction-band minimum, E , for electrons whose transmission coefficients are plotted in Fig. 8. All electrons have $E_z = E - E_c(\mathbf{k}_{\parallel}) \approx 0.01377 \text{ eV}$.

Curve	$k_x \text{ (\AA}^{-1}\text{)}$	$E \text{ (eV)}$
<i>A</i>	0.000	0.01377
<i>B</i>	0.010	0.02754
<i>C</i>	0.020	0.06383
<i>D</i>	0.030	0.11368
<i>E</i>	0.038	0.15891

is negative for all k_{\parallel} , and thus increasing k_{\parallel} for given k_c and k_w results in a transmission resonance at a lower bias.

Having established from the results presented in Fig. 8 and the J - V characteristics plotted in Fig. 6 that the one-dimensional approximation is woefully inadequate for this device, we examine the two-dimensional approximation (3). In Fig. 9 we graph the transmission of electrons lying near the bulk-emitter Fermi surface, with $k_{\parallel} = 0.04028 \text{ \AA}^{-1}$ and energy relative to the bulk-emitter conduction-band minimum, $E \approx 0.15864 \text{ eV}$, for varying directions of $\mathbf{k}_{\parallel} = k_{\parallel} \cos(\theta)\mathbf{e}_x + k_{\parallel} \sin(\theta)\mathbf{e}_y$. As with the previous device, there is some variation of peak position and width as the angle changes, but the spreading is not nearly as great as that shown in Fig. 8. This indicates that (3) is relatively speaking a much better approximation than (5) and is likely fairly good. At the very least, these results indicate that (3) represents a reasonable tradeoff between accuracy and effort, given the computational challenge posed by (1).

IV. SUMMARY AND CONCLUSIONS

Despite the great progress which has been made in modeling RTD's, most work on conduction-band tunneling still neglects the effects of nonzero k_{\parallel} . We have studied InAs/AlSb devices, which should be nearly ideal due to the large Γ - and X -valley barriers of AlSb relative to InAs, so that tunneling is mostly Γ like. Nevertheless, we have demonstrated here that including the explicit k_{\parallel} dependence of the transmission coefficient in J - V calculations for rather ordinary devices results in markedly different curves from those of calculations which neglect it. Previous work⁴ has shown that conduction-band non-parabolicity tends to spread out the transmission maxima for bulk emitter electrons of similar z energy but differing k_{\parallel} . Here we have seen that this spreading manifests itself in the J - V characteristics. We have also examined the angular dependence of the transmission coefficients for these devices, observing that while the transmission is not exactly isotropic, assuming it to be so is probably a good approximation, especially in light of the extraordinary computational effort necessary to include it. Thus we conclude that the one-dimensional approximation for the current density ought to be abandoned in favor of the two-dimensional approximation in most cases.

TABLE II. Tight-binding parameters (units are eV); the notation is that of Ref. 11.

Parameter	InAs	AlSb
$E(sa)$	-9.6081	-5.24996
$E(pa)$	0.9099	1.10214
$E(sc)$	-2.5519	-1.65016
$E(pc)$	3.7201	3.13774
$E(s^*a)$	7.4099	6.88214
$E(s^*c)$	6.7401	6.27574
$V(s,s)$	-5.4052	-5.6648
$V(x,x)$	1.8398	1.7199
$V(x,y)$	4.4693	3.6648
$V(sa,pc)$	3.3054	5.5000
$V(pa,sc)$	5.4389	6.2137
$V(s^*a,pc)$	3.3744	5.3000
$V(pa,s^*c)$	3.9097	5.2739

ACKNOWLEDGMENTS

We gratefully acknowledge discussions with R. E. Carnahan and K. P. Martin.

APPENDIX

In Table II we list the InAs and AlSb tight-binding parameters used in these calculations: they represent a compromise in fitting the masses and gaps at the Γ point and at the indirect minima at or near the X points. For InAs they reproduce $E_{g,dir} \approx 0.375 \text{ eV}$, $E_{g,ind} \approx 2.277 \text{ eV}$, and $m_{\Gamma}^* \approx 0.0266m_0$ and $m_X^* \approx 1.400m_0$, and for AlSb they reproduce $E_{g,dir} \approx 2.372 \text{ eV}$, $E_{g,ind} \approx 1.681 \text{ eV}$, $m_{\Gamma}^* \approx 0.136m_0$, and $m_X^* \approx 1.516m_0$. $E_{g,dir}$ denotes the energy difference between the conduction and valence bands at Γ , while $E_{g,ind}$ denotes the difference in energy between the conduction-band minimum along the $[100]$ directions and the valence-band maximum; m_0 denotes the free-electron mass and m_X^* the longitudinal X -valley mass. The AlSb-InAs conduction-band offset at Γ is taken to be approximately 2.119 eV. At the interfaces we use the InSb and AlAs anion-cation tight-binding parameters from Ref. 11.

¹K. V. Rousseau, K. L. Wang, and J. N. Schulman, *Superlatt. Microstruct.* **6**, 67 (1989); M. S. Kiledjian, J. N. Schulman, K. L. Wang, and K. V. Rousseau, *Surf. Sci.* **267**, 405 (1992); D. Z.-Y. Ting, E. T. Yu, and T. C. McGill, *Phys. Rev. B* **45**, 3576 (1992).
²M. S. Kiledjian, J. N. Schulman, K. L. Wang, and K. V. Rousseau, *Phys. Rev. B* **46**, 16012 (1992).
³D. J. Ben Daniel and C. B. Duke, *Phys. Rev.* **152**, 683 (1966).
⁴Timothy B. Boykin, R. E. Carnahan, and R. J. Higgins, *Phys. Rev. B* **48**, 14232 (1993).
⁵Material data are from *Semiconductors*, edited by O. Madelung, Landolt-Börnstein, New Series, Group III, Vol. 17, Pt. a (Springer-Verlag, Berlin, 1982), except the AlSb Γ -

valley effective mass, which is from S. M. Sze, *Physics of Semiconductor Devices*, 2nd ed. (Wiley, New York, 1981), p. 849.

⁶Timothy B. Boykin, *Appl. Phys. Lett.* **64**, 1529 (1994).

⁷L. F. Luo, R. Beresford, and W. I. Wang, *Appl. Phys. Lett.* **53**, 2320 (1988); D. H. Chow, J. R. Söderström, D. A. Collins, D. Z.-Y. Ting, E. T. Yu, and T. C. McGill, *Proc. SPIE* **1283**, 2 (1990); J. R. Söderström, E. R. Brown, C. D. Parker, L. J. Mahoney, J. Y. Yao, T. G. Andersson, and T. C. McGill, *Appl. Phys. Lett.* **58**, 275 (1991).

⁸R. E. Carnahan, M. A. Maldonado, K. P. Martin, A. Nogaret, R. J. Higgins, L. A. Cury, D. K. Maude, J. C. Portal, J. F. Chen, and A. Y. Cho, *Appl. Phys. Lett.* **62**, 1385 (1993).

- ⁹Bernider Brar, Herbert Kroemer, James Ibbetson, and John H. English, *Appl. Phys. Lett.* **62**, 3303 (1993).
- ¹⁰Timothy B. Boykin, R. E. Carnahan, and K. P. Martin, *Phys. Rev. B* **51**, 2273 (1995).
- ¹¹P. Vogl, Harold P. Hjalmarson, and John D. Dow, *J. Phys. Chem. Solids.* **44**, 365 (1983).
- ¹²D. H. Lee and J. D. Joannopoulos, *Phys. Rev. B* **23**, 4988 (1981); *J. Vac. Sci. Technol.* **19**, 355 (1981).
- ¹³Timothy B. Boykin, Jan P. A. van der Wagt, and James S. Harris, Jr., *Phys. Rev. B* **43**, 4777 (1991).
- ¹⁴D. Z.-Y. Ting, E. T. Yu, and T. C. McGill, *Appl. Phys. Lett.* **58**, 292 (1991); *Phys. Rev. B* **45**, 3583 (1992); D. Z.-Y. Ting and J. N. Schulman, *ibid.* **45**, 6282 (1992).
- ¹⁵In our parametrization of InAs there is a region of energy above the conduction-band minimum where the real parts of the k_z wave vectors of certain evanescent states reach the Brillouin zone edge; here the bulk InAs transfer matrix is numerically defective. We get around this problem by taking the expansion states from the diagonalization of a bulk InAs transfer matrix for energy 10 or 20 μ eV above or below this point. For all tight-binding J - V results, flux conservation for the calculated transmission coefficients was better than 10^{-6} ; that is, $R + T = 1.0 \pm \delta$, $0 \leq \delta \leq 10^{-6}$.
- ¹⁶The Poisson solution uses the bulk emitter quasi-Fermi level to the emitter side of the first barrier, and the bulk collector quasi-Fermi level for the remainder of the structure, which is the same as assuming that the first barrier blocks all of the current.
- ¹⁷William H. Press, Brian P. Flannery, Saul A. Teukolsky, and William T. Vetterling, *Numerical Recipes in C: the Art of Scientific Computing* (Cambridge University Press, New York, 1988), pp. 566–580.
- ¹⁸The conduction band of GaAs is often modeled with an expression of this form; see Jasprit Singh, *Physics of Semiconductors and Their Heterostructures* (McGraw-Hill, New York, 1993), p. 166. The conduction band of InAs is also readily described by this form.